Supplement of Geosci. Model Dev., 19, 9019–9033, 2026
https://doi.org/10.5194/gmd-19-9019-2026-supplement

Geoscientific Model Development
Open Access

Supplement of

Consideration of radiation absorption by stems in forests for microclimate modeling

Martin Béland et al.

Correspondence to: Martin Béland (martin.beland@scg.ulaval.ca)

Contents of this file

Text S1
Figures S1 to S12

Introduction

The first section (S1) provides the complete set of modified equations for the Norman model presented in the main paper, which includes radiation absorption by wood and a modification to clumped layers scattering coefficient to account for multiple scattering.

The second section presents additional figures (S1 – S12) comparing model outputs for all variables and all sites complementing those presented in the paper.

S1. Mathematical formulation of Norman's model modified for wood absorption and recollision probability. Tridiagonal solution equations adapted from Bonan (2019)

The cumulative transmittance of direct beam radiation in layer i is:

$$T_{b,i}=\begin{cases} 1 & i=N \\ \prod_{j=i+1}^{N} exp\left(-\frac{G_{l,j}\Omega_{l,j}\Delta LAI_j+2\cdot G_{w,j}\Omega_{w,j}\Delta WAI_j}{\cos\theta}\right) & i\le N-1 \end{cases}$$

And the direct beam radiation transmittance through layer i+1 is:

$$\tau_{b,i}=exp\left(-\frac{G_{l,i}\Omega_{l,i}\Delta LAI_i+2\cdot G_{w,i}\Omega_{w,i}\Delta WAI_i}{\cos\theta}\right)$$

The diffuse radiation transmittance through layer i is:

$$\tau_{d,i}=2\sum_{k=1}^{90} exp\left[-\frac{G_{l,k,i}\Omega_{l,i}LAI_i+2\cdot G_{w,k,i}\Omega_{w,i}WAI_i}{\cos Z_k}\right]\sin Z_k\cos Z_k\Delta Z_k$$

The fractions of intercepted diffuse radiation by leaves and wood in layer i are respectively:

$$\mathrm{frac}_{d,l,i} = 2\sum_{k=1}^{90} \frac{G_{l,i,k}\Omega_{l,i}\Delta LAI_i}{G_{l,i,k}\Omega_{l,i}\Delta LAI_i + 2\cdot G_{w,i,k}\Omega_{w,i}\Delta WAI_i} \sin Z_k \cos Z_k \Delta Z_k$$

Equation 1

And

$$\mathrm{frac}_{d,w,i} = 2\sum_{k=1}^{90} \frac{2\cdot G_{w,i,k}\Omega_{w,i}\Delta WAI_i}{G_{l,i,k}\Omega_{l,i}\Delta LAI_i + 2\cdot G_{w,i,k}\Omega_{w,i}\Delta WAI_i} \sin Z_k \cos Z_k \Delta Z_k$$

Equation 2

Where k represents the numerical approximation for 90 sky zones from where radiation is incident, Z_k are the individual sky zones, and ΔZ is π / 180. The cumulative effective element area index is:

$$Ceff\,EAI = \frac{\Delta LAI\cdot \Omega_l \cdot G_l + \Delta WAI \cdot \Omega_w \cdot 2\cdot G_w}{\cos\theta}$$

And the fraction of sunlit leaf area and wood area in layer i (which are the same for a given layer) is:

$$f\,sun_i = \frac{exp\left(-Ceff\,EAI_{i+1}\right) - exp\left(-Ceff\,EAI_i\right)}{\frac{LAI_i \cdot G_{l,i} + WAI_i \cdot 2 \cdot G_{w,i}}{\cos\theta}}$$

The terms of the tridiagonal system presented in Bonan (2019) become:

$$a_i = f_{\ i+1} = B - \frac{A^2}{B}$$

$$b_i = e_{i+1} = \frac{A}{B}$$

With

$$A = \tau_{d,i+1} + \left(1 - \tau_{d,i+1}\right)\cdot f\,rac_{l,i+1} \cdot \tau'_{l,i+1} + \left(1 - \tau_{d,i+1}\right) \cdot f\,rac_{w,i+1} \cdot \frac{\rho_w}{2}$$

And

$$B = \left(1 - \tau_{d,i+1}\right) \cdot frac_{l,i+1} \cdot \rho'_{l,i+1} + \left(1 - \tau_{d,i+1}\right) \cdot frac_{w,i+1} \cdot \frac{\rho_w}{2}$$

Where τ'_l and ρ'_l are respectively the leaf transmittance and reflectance modified to account for the decreased scattering of clumped leaf shoots following increased recollision probability (see section 2.3). ρ_w is the wood reflectance, here divided by 2 assuming half of the reflectance is directed upward and half downward.

Other tridiagonal terms are:

$$c_i = I^{\downarrow}_{sky,b} \cdot T_{b,i} \cdot \left(\left(1 - \tau_{b,i}\right) \cdot frac_{l,i} \cdot \left(\rho'_{l,i} - \tau'_{l,i} \cdot e_i\right) + \left(1 - \tau_{b,i}\right) \cdot frac_{w,i} \cdot \frac{\rho_w}{2}\left(1 - e_i\right)\right)$$

and

$$d_i = I^{\downarrow}_{sky,b} \cdot T_{b,i+1} \cdot \left(\left(1 - \tau_{b,i+1}\right) \cdot frac_{l,i+1} \cdot \left(\tau'_{l,i+1} - \rho'_{l,i+1} \cdot b_i\right) + \left(1 - \tau_{b,i+1}\right) \cdot frac_{w,i+1} \cdot \frac{\rho_w}{2}\left(1 - b_i\right)\right)$$

Where $I^{\downarrow}_{sky,b}$ is the incident direct beam radiation at the top of the canopy.

The diffuse and direct beam fluxes absorbed by leaves per ground area in layer i are respectively:

$$\overrightarrow{I_{cd,l,i}} = \left(I^{\downarrow}_i + I^{\uparrow}_{i-1}\right) \cdot \left(1 - \tau_{d,i}\right) \cdot frac_{l,i} \cdot \left(1 - \omega'_{l,i}\right) + \left(I^{\downarrow}_{sky,b} T_{b,i}\right) \cdot \left(1 - \tau_{b,i}\right) \cdot frac_{l,i} \cdot \left(\omega_{l,i} - \omega'_{l,i}\right)$$

And

$$\overrightarrow{I_{cb,l,i}} = \left(I^{\downarrow}_{sky,b} T_{b,i}\right) \cdot \left(1 - \tau_{b,i}\right) \cdot frac_{l,i} \cdot \left(1 - \omega_{l,i}\right)$$

And the diffuse and direct beam fluxes absorbed by wood in layer i are:

$$\overrightarrow{I_{cd,w,i}} = \left(I^{\downarrow}_i + I^{\uparrow}_{i-1}\right) \cdot \left(1 - \tau_{d,i}\right) \cdot frac_{w,i} \cdot \left(1 - \omega_{w,i}\right)$$

And

$$\overrightarrow{I_{cb,w,i}} = \left(I^{\downarrow}_{sky,b} T_{b,i}\right) \cdot \left(1 - \tau_{b,i}\right) \cdot frac_{w,i} \cdot \left(1 - \omega_{w,i}\right)$$

For **longwave radiation** leaf emissivity is 0.98, leaf forward scattering ρ_l and forward scattering τ_l were both set at 0.01. For wood, emissivity is around 0.92 and we set reflectance and transmittance in equal proportion a 0.04:

$$\rho_w = \tau_w = \frac{1 - \varepsilon_w}{2} = 0.04$$

For longwave, $frac_{l,i}$ and $frac_{w,i}$ refer to fractions of intercepted diffuse radiation following Equation 1 and Equation 2 above. Again, starting from the equations developed in Bonan (2019), we have the longwave radiation emitted by layer i:

$$\varepsilon_l \sigma T_{l,i}^4 \left(1 - \tau_{d,i}\right) \cdot frac_{l,i} + \varepsilon_w \sigma T_{w,i}^4 \left(1 - \tau_{d,i}\right) \cdot frac_{w,i}$$

And the tridiagonal terms:

$$a_i = f_{i+1} = B - \frac{A^2}{B}$$

$$b_i = e_{i+1} = \frac{A}{B}$$

With

$$A = \tau_{d,i+1} + \left(\left(1 - \tau_{d,i+1}\right) \cdot frac_{l,i+1} \cdot \tau_{l,i+1} + \left(1 - \tau_{d,i+1}\right) \cdot frac_{w,i+1} \cdot \rho_{w,i+1}\right)$$

$$B = \left(1 - \tau_{d,i+1}\right) \cdot frac_{l,i+1} \cdot \rho_{l,i+1} + \left(1 - \tau_{d,i+1}\right) \cdot frac_{w,i+1} \cdot \rho_{w,i+1}$$

And

$$c_i = \left(1 - e_i\right)\left(\varepsilon_l \sigma T_{l,i}^4 \left(1 - \tau_{d,i}\right) \cdot frac_{l,i} + \varepsilon_w \sigma T_{w,i}^4 \left(1 - \tau_{d,i}\right) \cdot frac_{w,i}\right)$$

$$d_i = \left(1 - b_i\right)\left(\varepsilon_l \sigma T_{l,i+1}^4 \left(1 - \tau_{d,i+1}\right) \cdot frac_{l,i+1} + \varepsilon_w \sigma T_{w,i+1}^4 \left(1 - \tau_{d,i+1}\right) \cdot frac_{w,i+1}\right)$$

The net longwave fluxes per ground area for leaves and wood are :

$$\overrightarrow{L_{l,i}} = \varepsilon_l \cdot \left(L_i^{\downarrow} + L_{i-1}^{\uparrow}\right)\left(1 - \tau_{d,i}\right) - 2 \cdot \varepsilon_l \sigma T_{l,i}^4 \left(1 - \tau_{d,i}\right) \cdot frac_{l,i}$$

$$\overrightarrow{L_{w,i}} = \varepsilon_w \cdot \left(L_i^{\downarrow} + L_{i-1}^{\uparrow}\right)\left(1 - \tau_{d,i}\right) - 2 \cdot \varepsilon_w \sigma T_{w,i}^4 \left(1 - \tau_{d,i}\right) \cdot frac_{w,i}$$

In this study, we indirectly accounted for multiple scattering within clumped shoots in the Norman model by modifying a clumped layer's scattering coefficient following the approximation proposed in Smolander and Stenberg (2003). This approach is based on the assumptions that (1) the shoot clumping index as defined in Béland and Baldocchi (2020) for broadleaf shoots is equivalent to the needleleaf shoot shading factor as defined in Smolander and Stenberg (2003), and (2) the relation between shoot clumping index and recollision probability (recollision probability being equal to one minus the clumping index) is a good enough approximation to account for multiple scattering within a clumped element volume. The effect of the recollision probability on the radiative transfer can then be accounted for by modifying the absorptance of a clumped area (A_{sh}) using:

$$A_{sh} = \frac{1-\omega}{1-(1-\Omega)\cdot\omega}$$

Equation 3

Where ω is the leaf-level scattering ($\rho+\tau$, where ρ is leaf reflectance, and τ leaf transmittance), and Ω is the layer leaf clumping index which changes vertically in the canopy. The scattering coefficient for a clumped layer (ω') is 1-A_{sh}. Since the Norman model does not enable multiple scattering within a layer, the leaf-level reflectance and transmittance are here modified to account for the decreased scattering of clumped leaf shoots following: $\rho' = (\rho / \omega) \cdot \omega'$ and $\tau' = (\tau / \omega) \cdot \omega'$.

Comparison between models

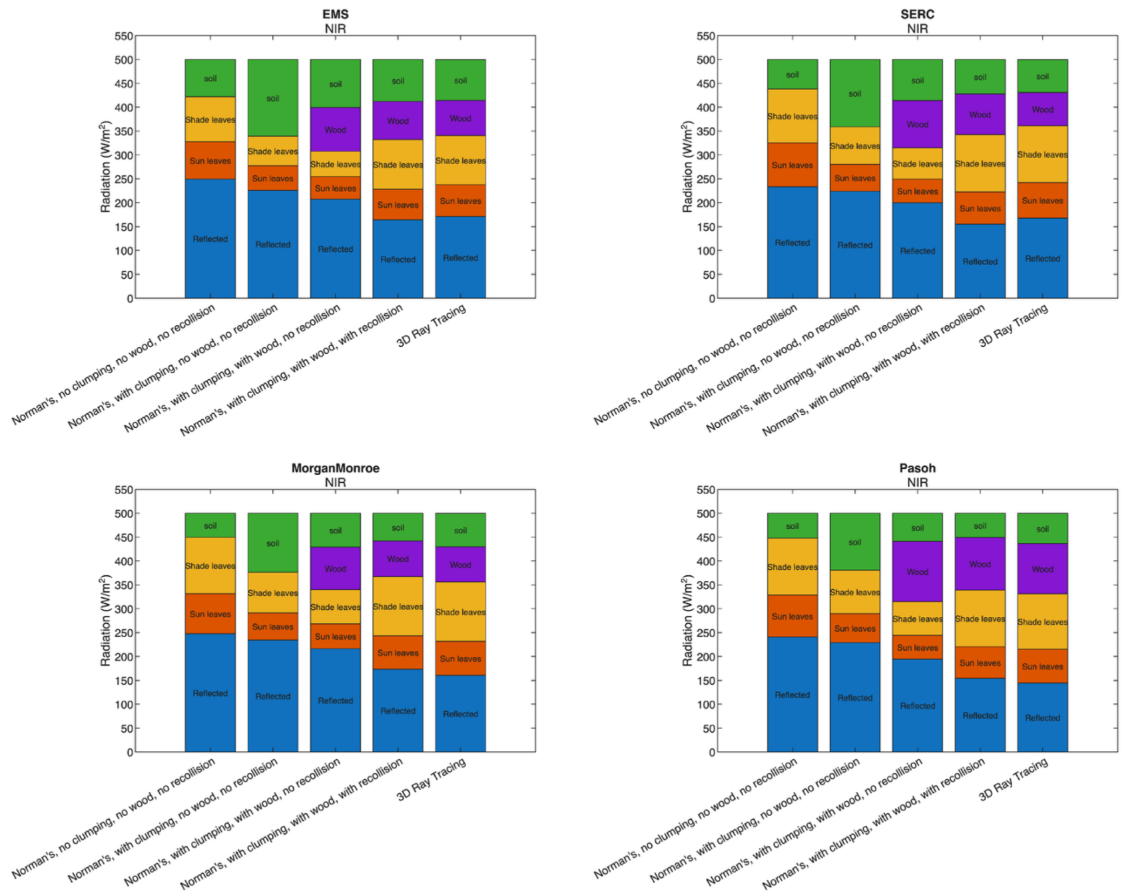

Figure S 1: Budget for the proportions of NIR reflected, and absorbed by sunlit and shaded leaves, by wood and soil, simulated using the Norman model with four different configurations and the FLiESvox 3D ray tracing model.

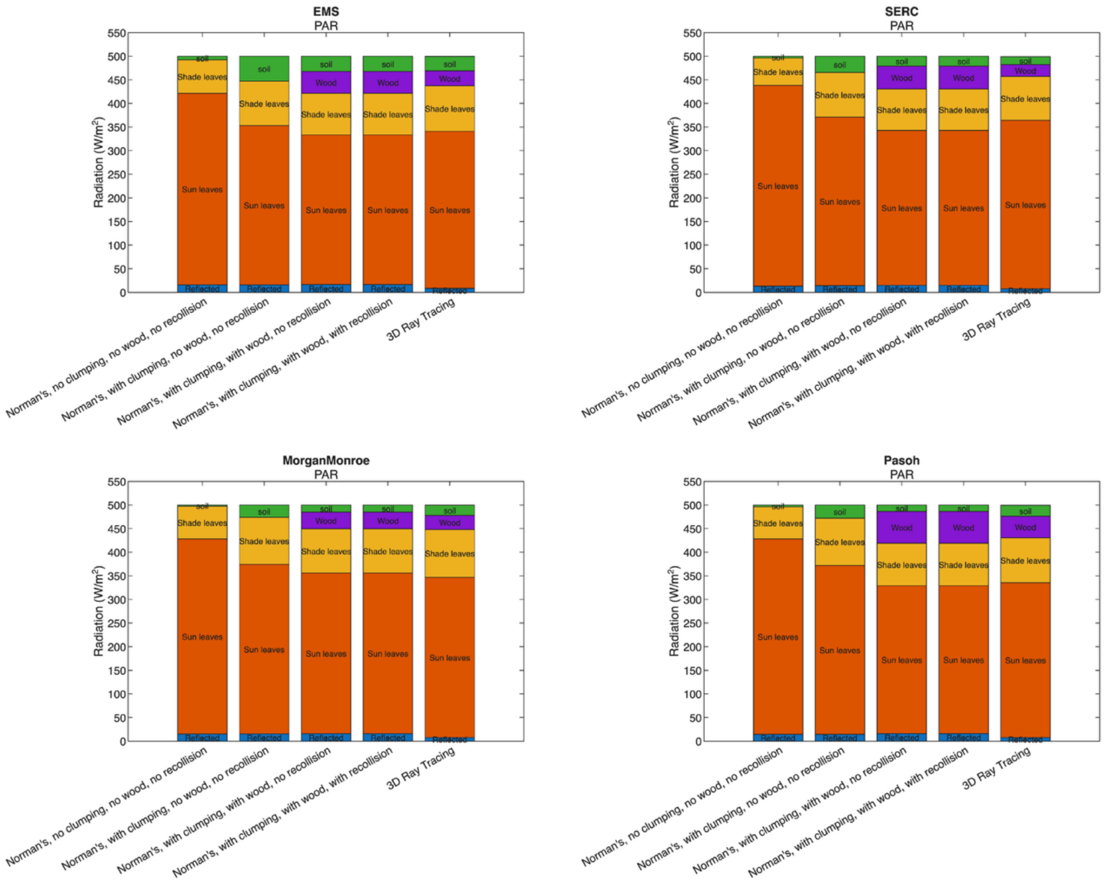

Figure S 2: Budget for the proportions of PAR reflected, and absorbed by sunlit and shaded leaves, by wood and soil, simulated using the Norman model with four different configurations and the FLiESvox 3D ray tracing model.

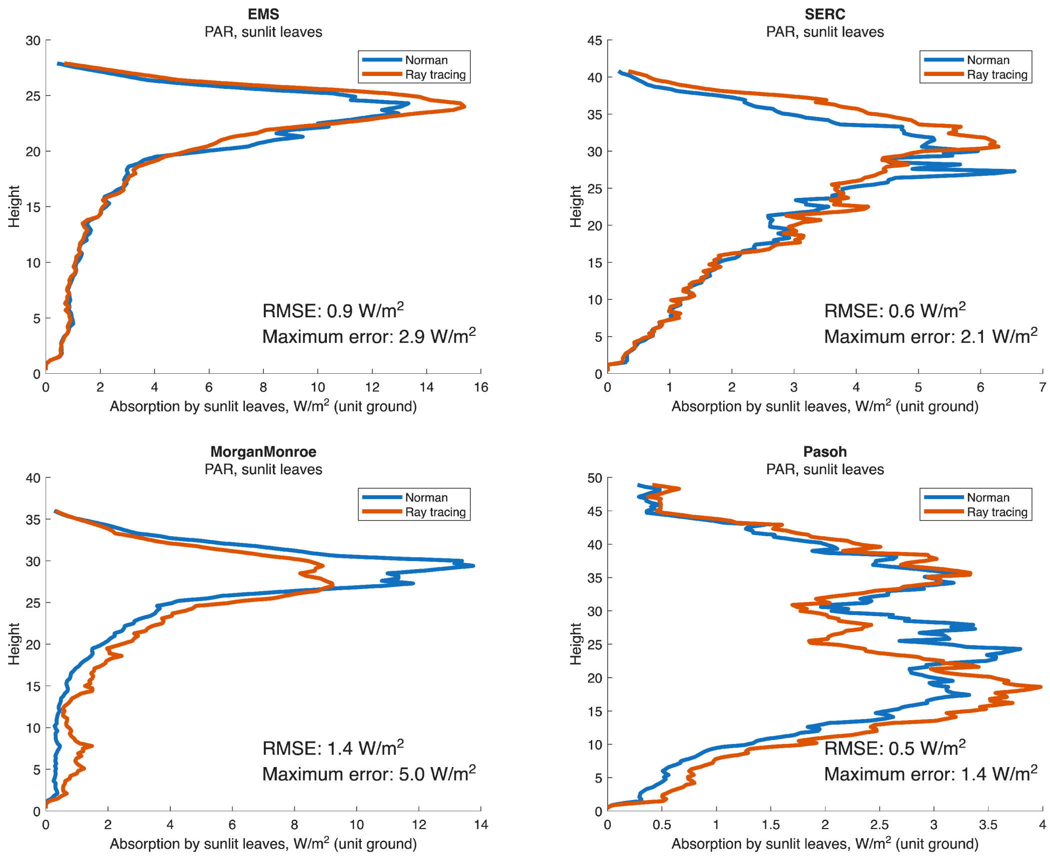

Figure S 3: Vertical profiles of PAR absorbed by sunlit leaves for the modified Norman (all modifications presented in paper) and FLiESvox models

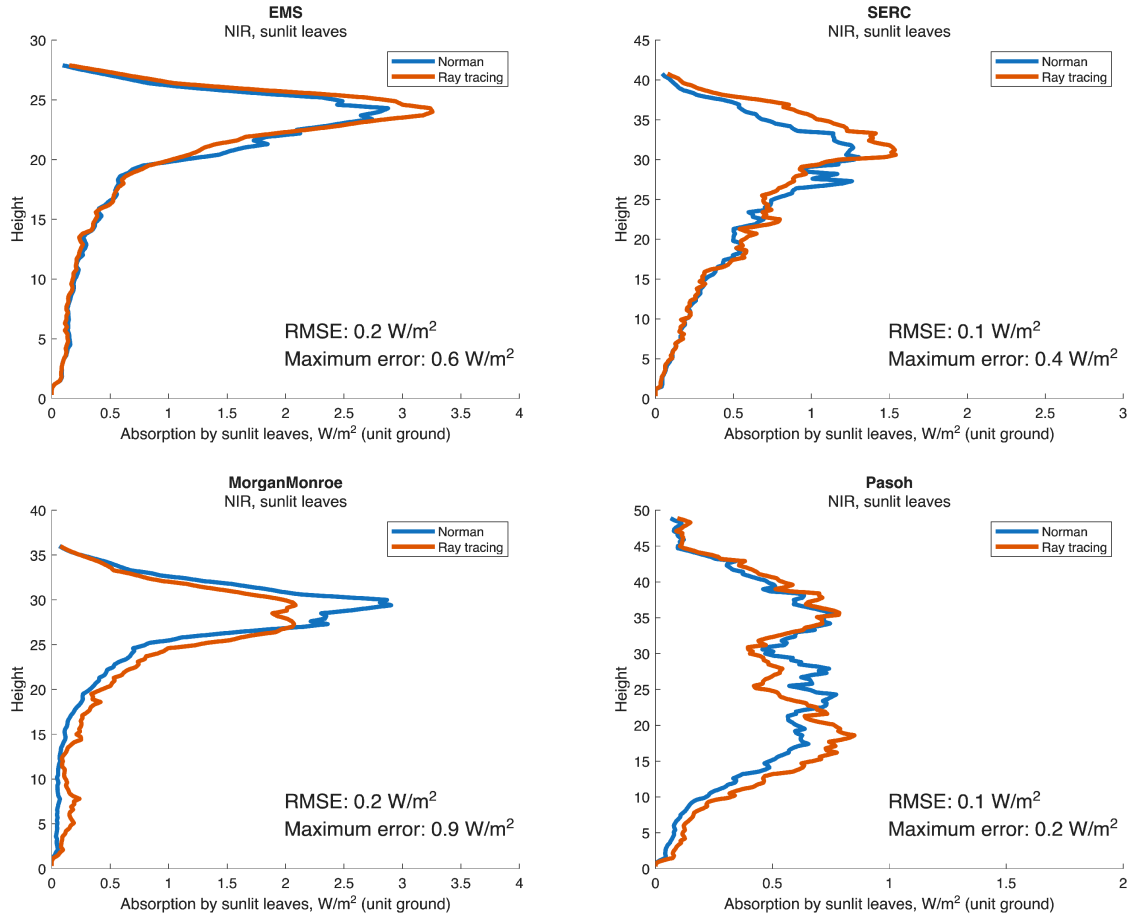

Figure S 4: Vertical profiles of NIR absorbed by sunlit leaves for the modified Norman (all modifications presented in paper) and FLiESvox models

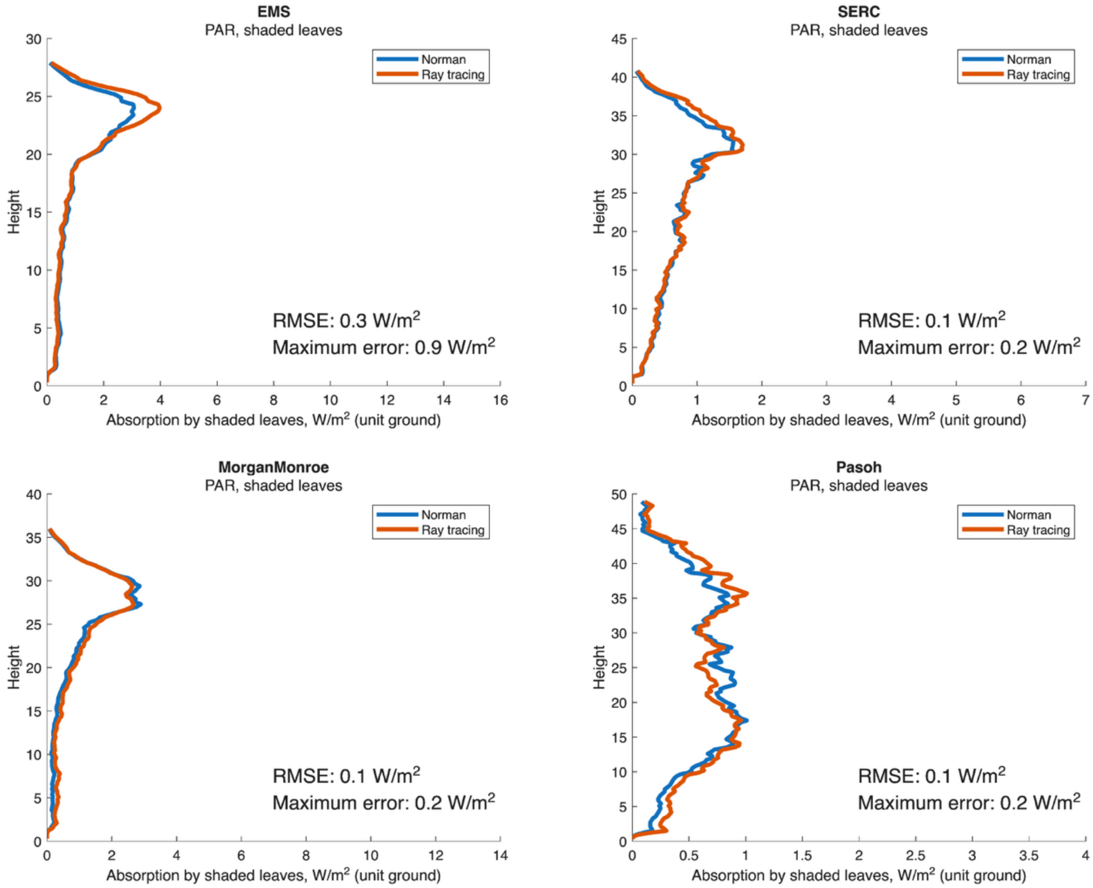

Figure S 5: Vertical profiles of PAR absorbed by shaded leaves for the modified Norman (all modifications presented in paper) and FLiESvox models

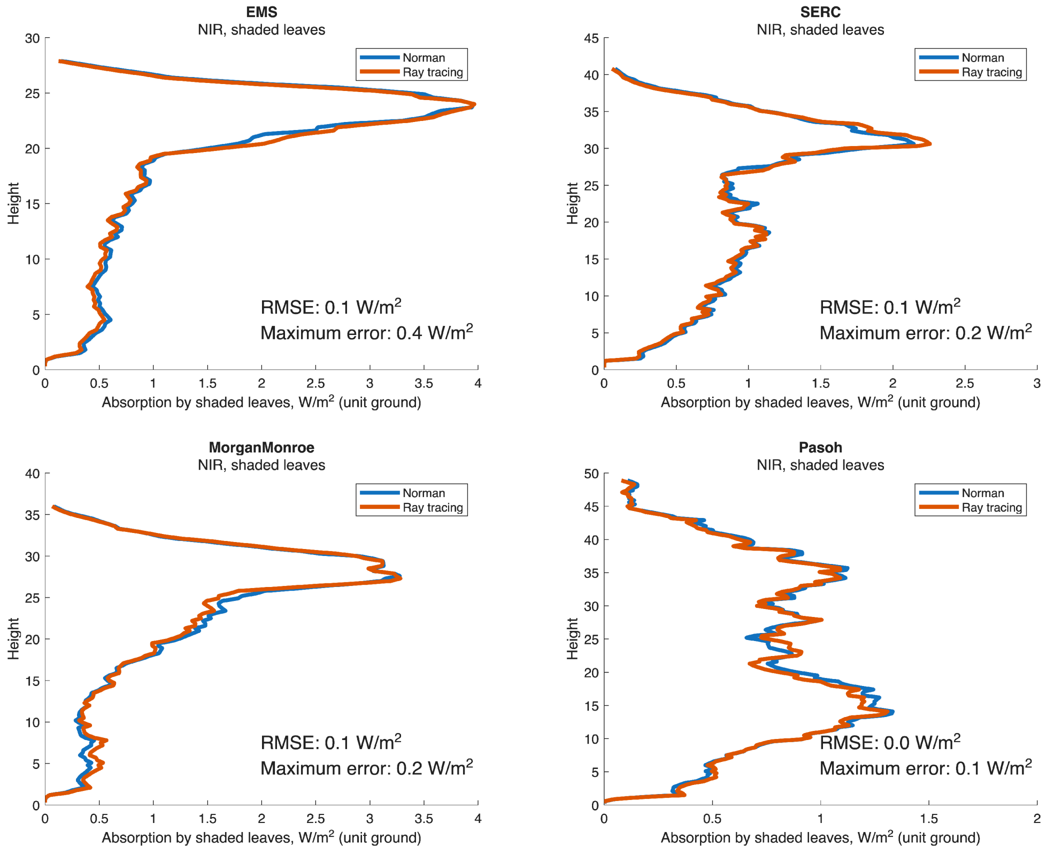

Figure S 6: Vertical profiles of NIR absorbed by shaded leaves for the modified Norman (all modifications presented in paper) and FLiESvox models

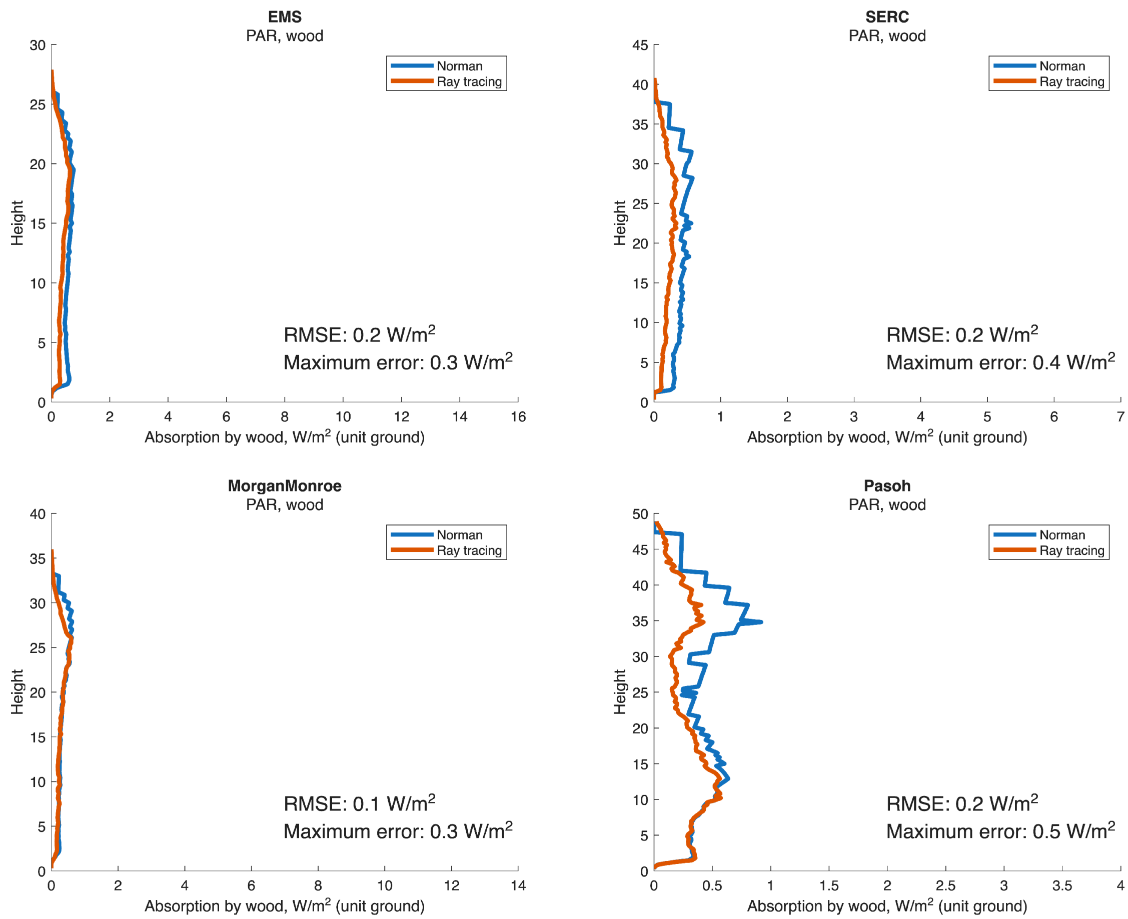

Figure S 7: Vertical profiles of PAR absorbed by wood for the modified Norman (all modifications presented in paper) and FLiESvox models

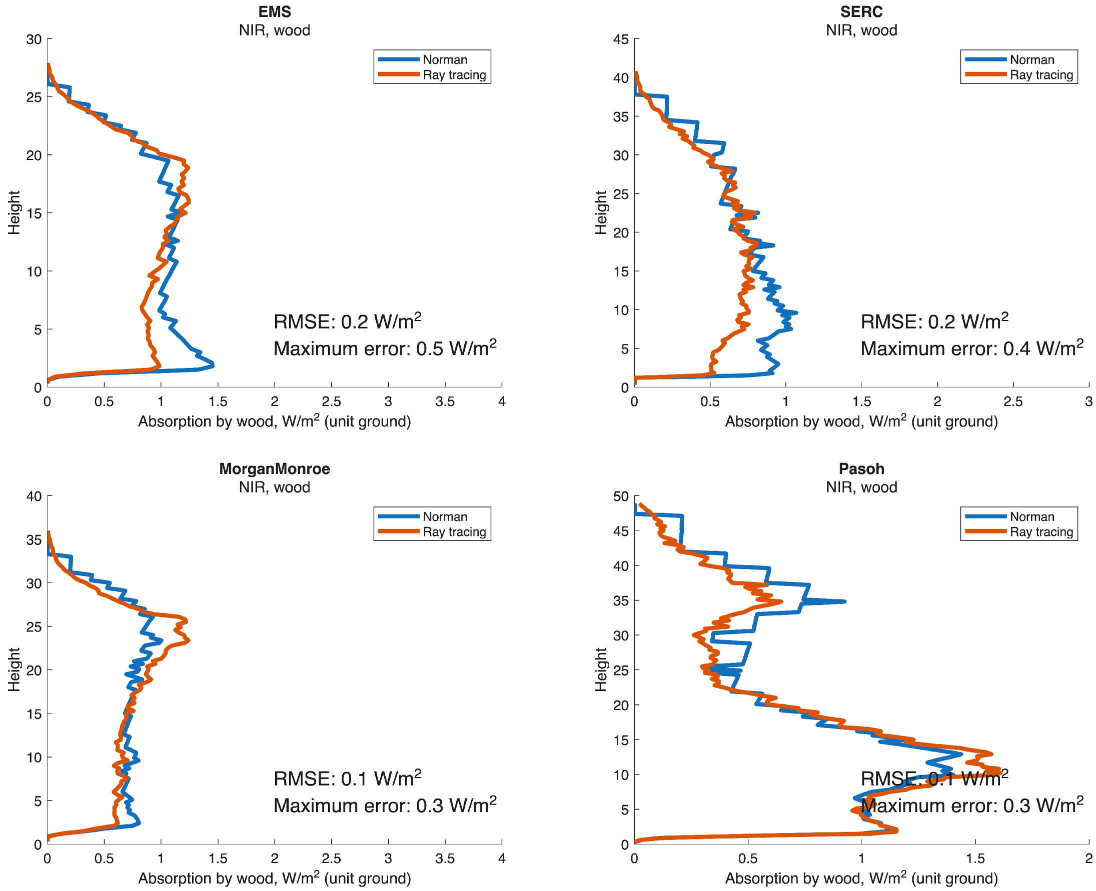

Figure S 8: Vertical profiles of NIR absorbed by wood for the modified Norman (all modifications presented in paper) and FLiESvox models

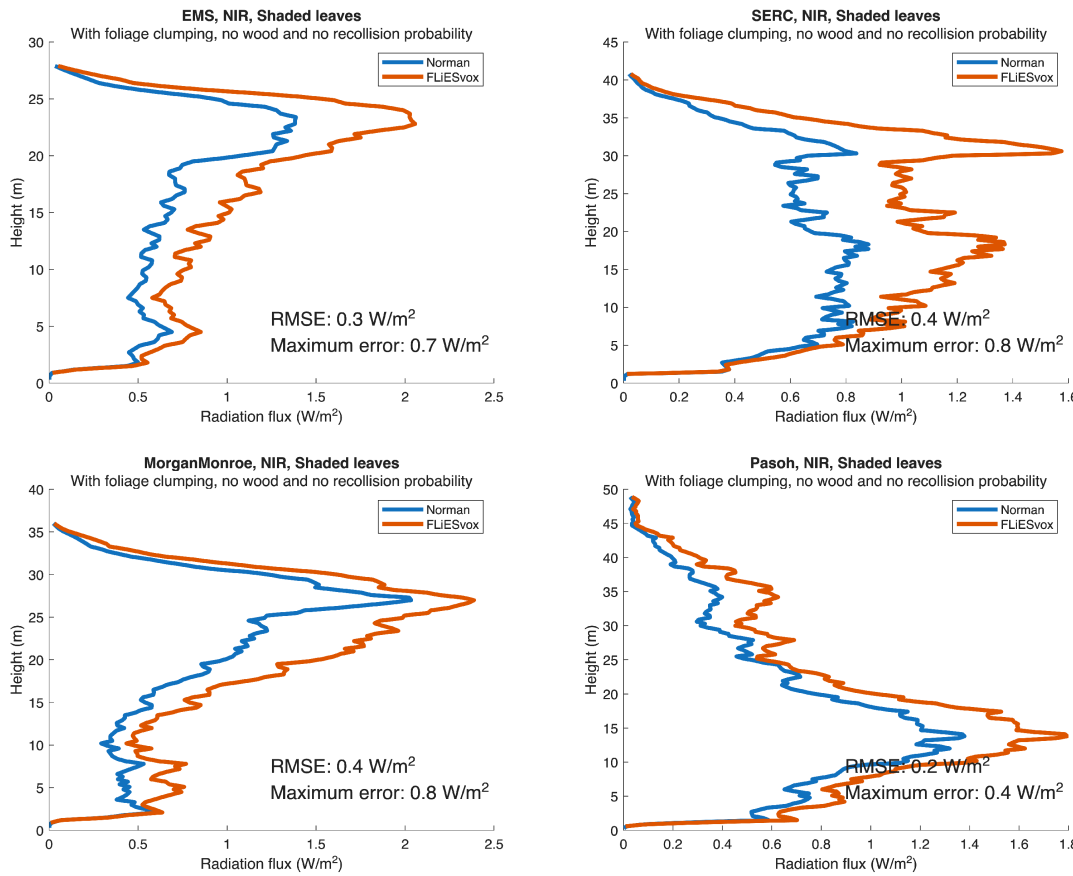

Figure S 9: Evaluation of the addition of leaf clumping to the Norman model by comparison to the 3D ray tracing model estimates for all sites. Both models do not consider wood nor recollision probability. Shown here is NIR absorbed by shaded leaves.

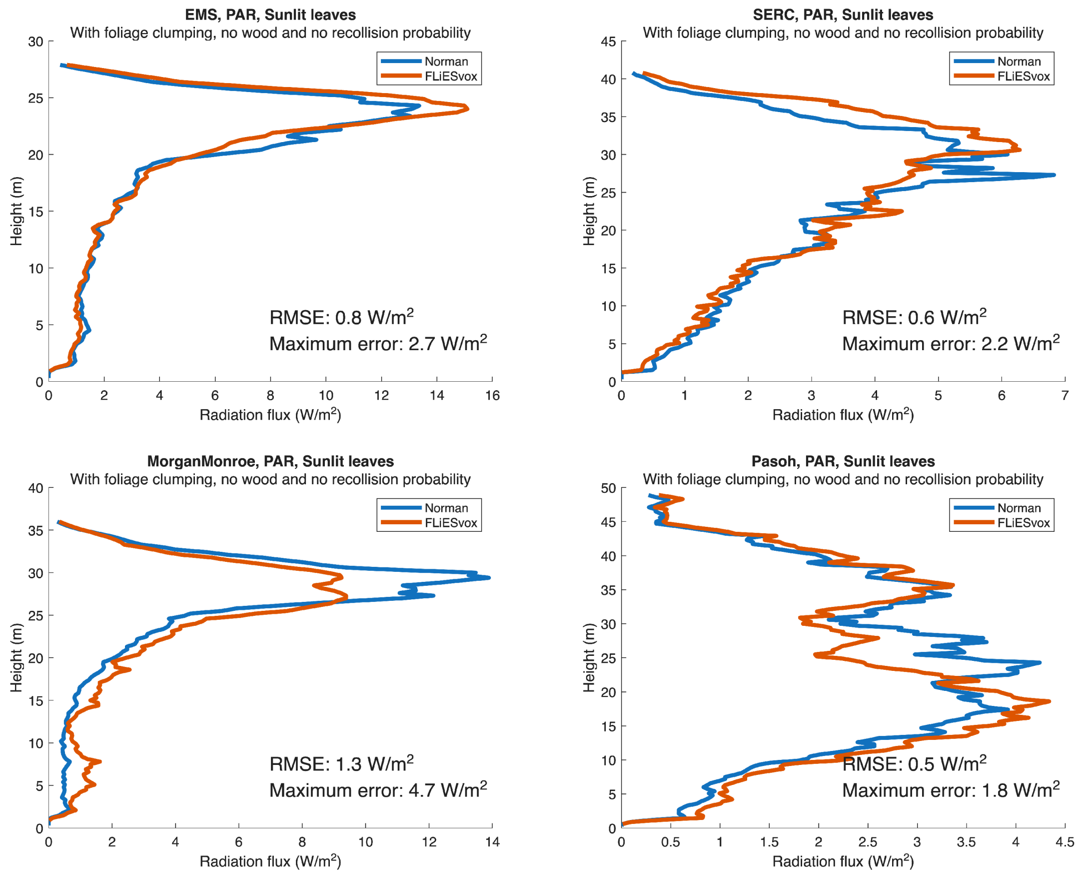

Figure S 10: Evaluation of the addition of leaf clumping to the Norman model by comparison to the 3D ray tracing model estimates for all sites. Both models do not consider wood nor recollision probability. Shown here is PAR absorbed by sunlit leaves.

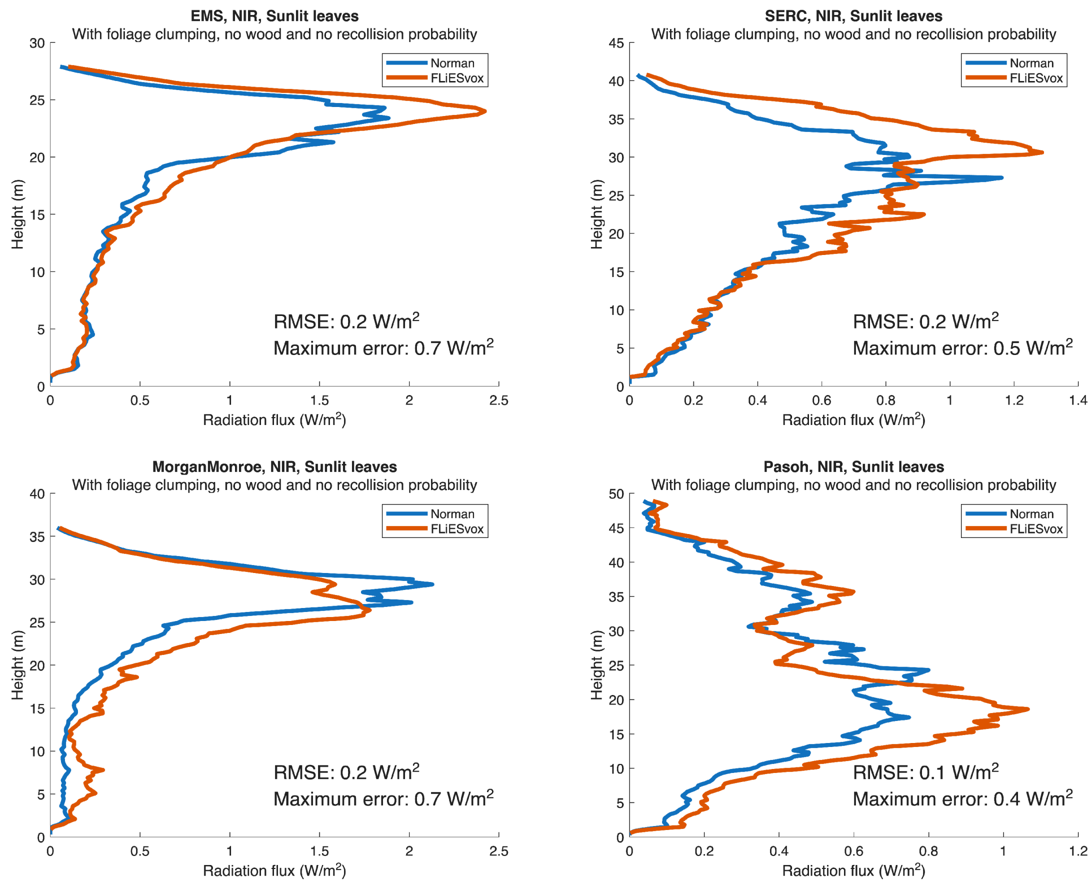

Figure S 11 Evaluation of the addition of leaf clumping to the Norman model by comparison to the 3D ray tracing model estimates for all sites. Both models do not consider wood nor recollision probability. Shown here is NIR absorbed by sunlit leaves.

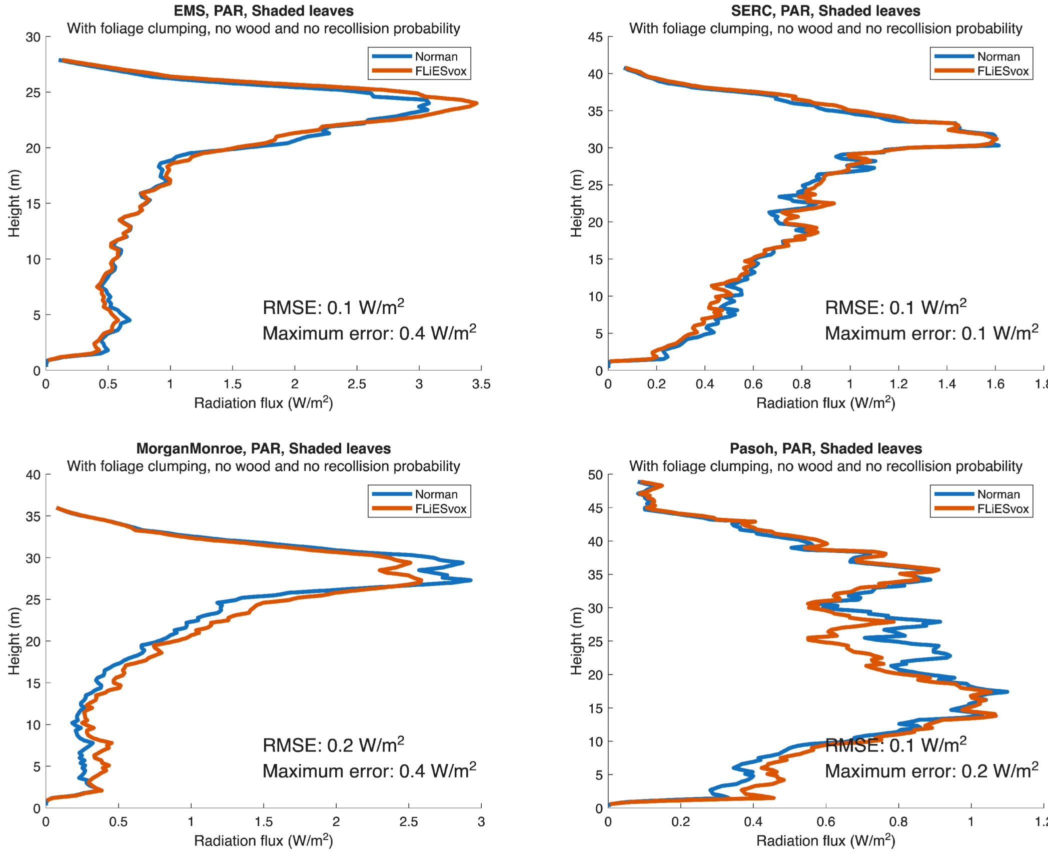

Figure S 12: Evaluation of the addition of leaf clumping to the Norman model by comparison to the 3D ray tracing model estimates for all sites. Both models do not consider wood nor recollision probability. Shown here is PAR absorbed by shaded leaves.

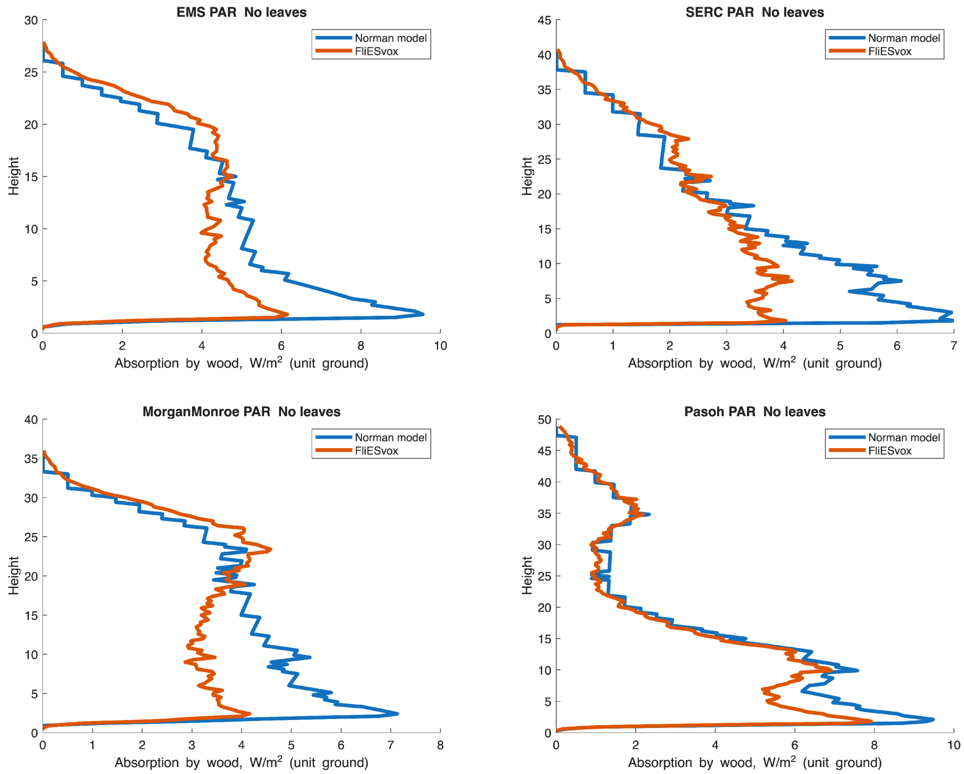

Figure S 13: Vertical profiles of PAR absorbed by wood for the modified Norman (all modifications presented in paper) and FLiESvox models in the particular case where there are no leaves in the canopy. 1000 W/m^2 of incoming radiation

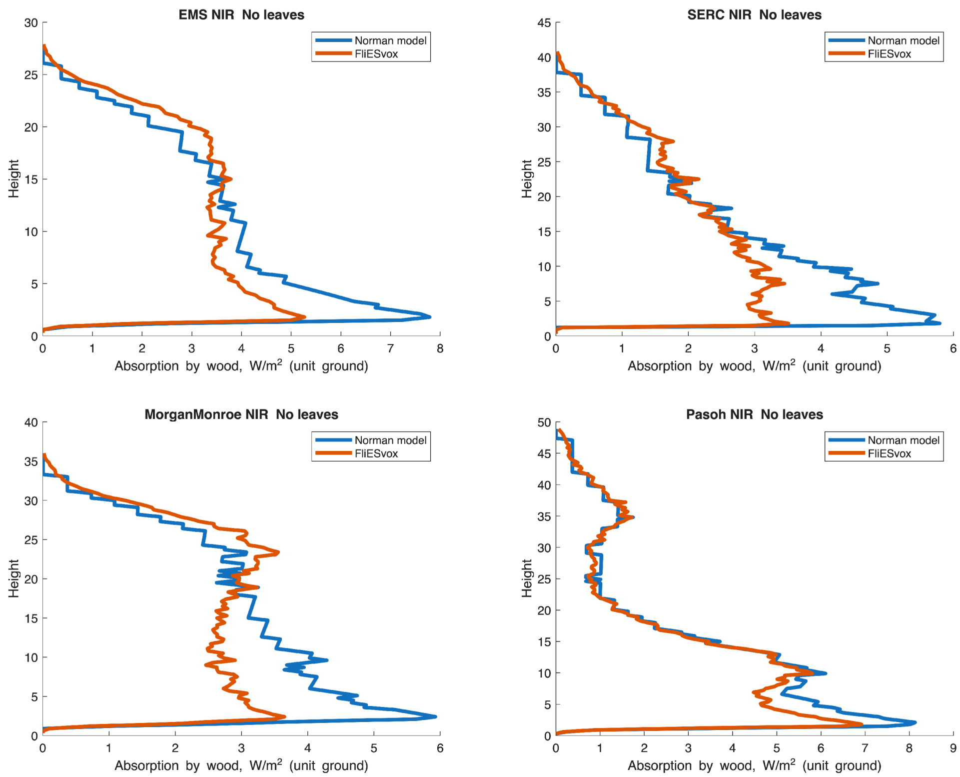

Figure S 14: Vertical profiles of NIR absorbed by wood for the modified Norman (all modifications presented in paper) and FLiESvox models in the particular case where there are no leaves in the canopy. 1000 W/m² of incoming radiation

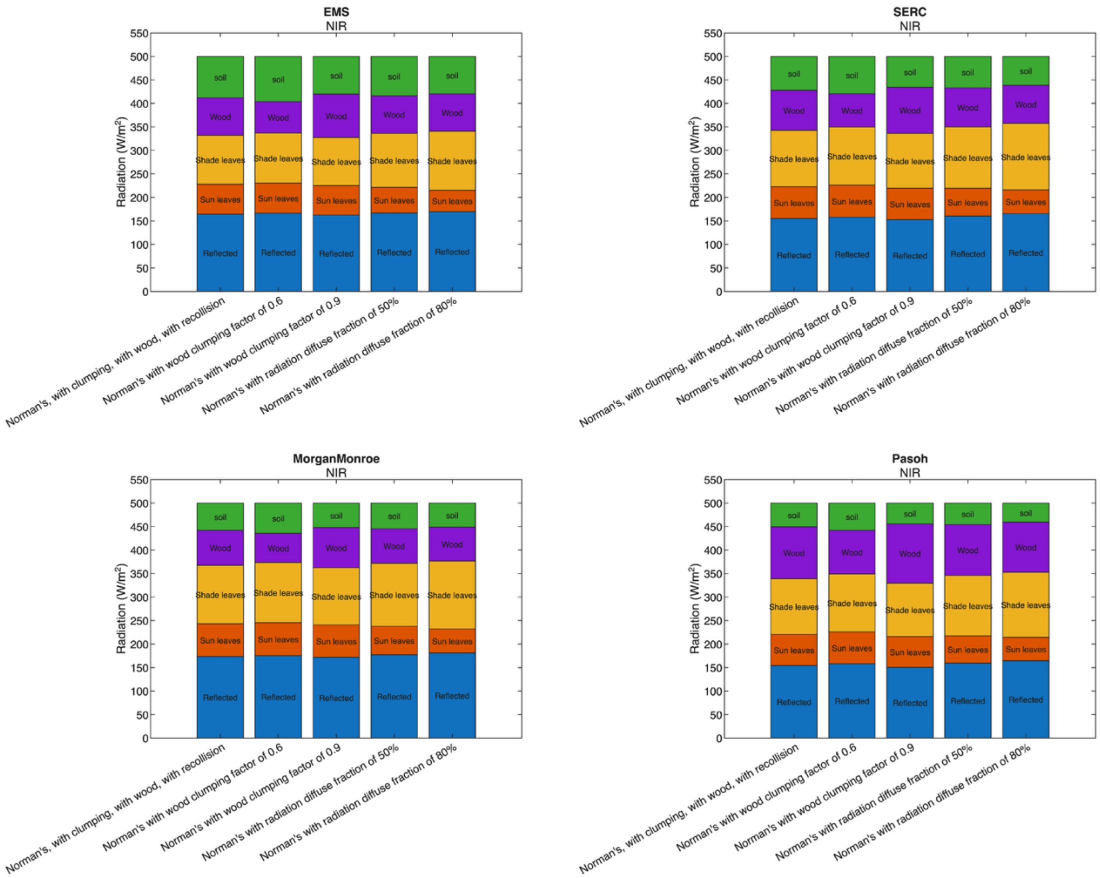

Figure S 15: Model sensitivity to wood clumping factor and incoming radiation diffuse fraction. Figure shows the budgets at each site for the proportions of NIR reflected, and absorbed by sunlit and shaded leaves, by wood and soil, simulated using the Norman model with five different configurations, including variations in wood clumping factor and diffuse fraction.

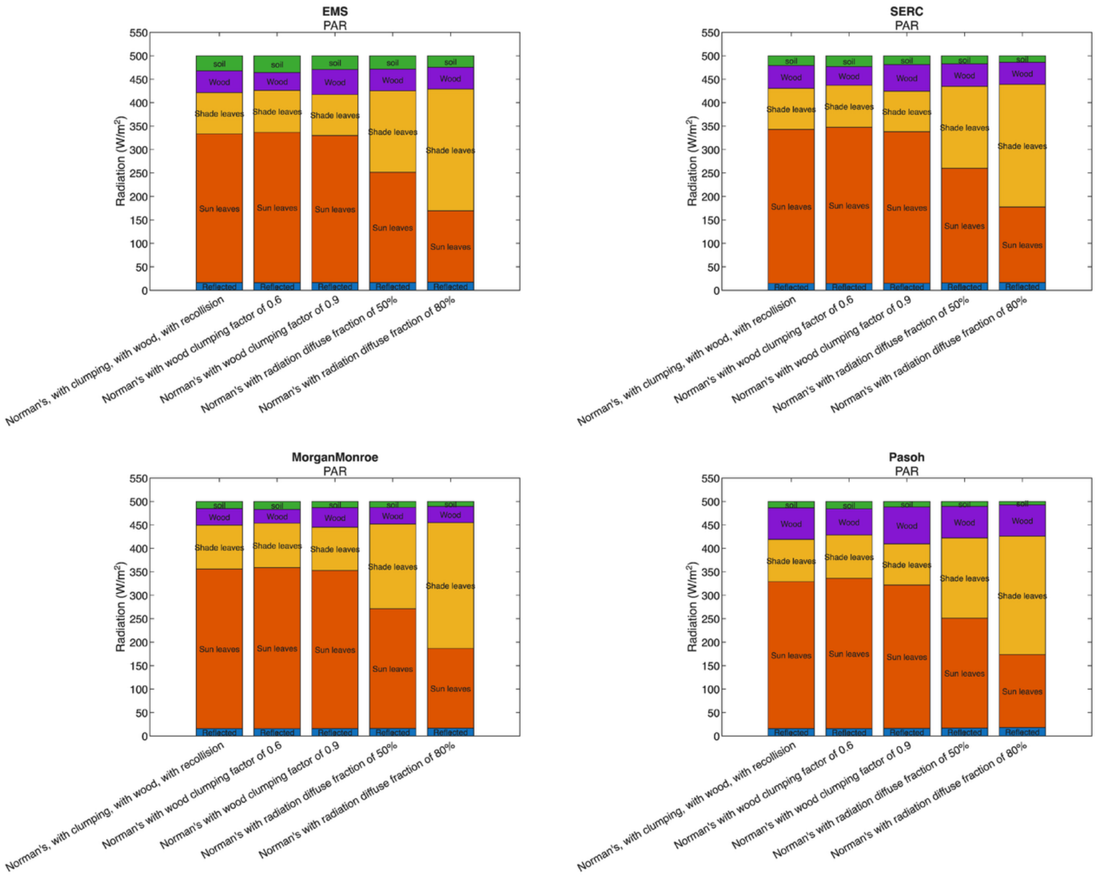

Figure S 16: Model sensitivity to wood clumping factor and incoming radiation diffuse fraction. Figure shows the budgets at each site for the proportions of PAR reflected, and absorbed by sunlit and shaded leaves, by wood and soil, simulated using the Norman model with five different configurations, including variations in wood clumping factor and diffuse fraction.

References

1. Béland, M. and Baldocchi, D., 2020. Is foliage clumping an outcome of resource limitations within forests? Agric. For. Meteorol., 295: 108185.
2. Bonan, G., 2019. Climate change and terrestrial ecosystem modeling. Cambridge University Press.
3. Smolander, S. and Stenberg, P., 2003. A method to account for shoot scale clumping in coniferous canopy reflectance models. Remote Sens. Environ., 88(4): 363-373.